HHS Public Access

Author manuscript

J Control Release. Author manuscript; available in PMC 2023 September 01.

Published in final edited form as:

J Control Release. 2022 September ; 349: 413–424. doi:10.1016/j.jconrel.2022.07.008.

Indocarbocyanine nanoparticles extravasate and distribute better than liposomes in brain tumors

Irina V. Balyasnikova[1,2,*], **Markella Zannikou**[1,2,#], **Guankui Wang**[3,4,#], **Yue Li**[3,4], **Joseph T. Duffy**[1,2], **Rebecca N. Levine**[1,2], **Maggie Seblani**[1,2,5], **Hanmant Gaikwad**[3,4], **Dmitri Simberg**[3,4,*]

[1]Department of Neurological Surgery, Feinberg School of Medicine, Northwestern University, Chicago, IL 60611, USA

[2]Northwestern Medicine Malnati Brain Tumor Institute of the Lurie Comprehensive Cancer Center, Feinberg School of Medicine, Northwestern University, Chicago, IL 60611, USA

[3]Department of Pharmaceutical Sciences, Skaggs School of Pharmacy and Pharmaceutical Sciences, University of Colorado Anschutz Medical Campus, Aurora, CO 80045, USA

[4]Colorado Center for Nanomedicine and Nanosafety, University of Colorado Anschutz Medical Campus, Aurora, CO 80045, USA

[5]Ann & Robert H. Lurie Children's Hospital of Chicago, Chicago, IL 60611USA

Abstract

Glioblastoma (GBM) is the most devastating and aggressive brain tumor in adults. Hidden behind the blood-brain and blood-tumor barriers (BBTB), this invasive type of brain tumor is not readily accessible to nano-sized particles. Here we demonstrate that fluorescent indocarbocyanine lipids (ICLs: DiD, DiI) formulated in PEGylated lipid nanoparticle (PLN) exhibit highly efficient penetration and accumulation in GBM. PLN-formulated ICLs demonstrated more efficient penetration in GBM spheroids and organoids *in vitro* than liposomal ICLs. Over 82% of the tumor's extravascular area was positive for ICL fluorescence in the PLN group versus 13% in the liposomal group just one hour post-systemic injection in the intracranial GBM model. Forty-eight hours post-injection, PLN-formulated ICLs accumulated in 95% of tumor myeloid-derived suppressor cells and macrophages, 70% of tumor regulatory T cells, 50% of tumor-associated microglia, and 65% of non-immune cells. PLN-formulated ICLs extravasated better than PEGylated liposomal doxorubicin and fluorescent dextran and efficiently accumulated in invasive tumor margins and brain-invading cells. While liposomes were stable in serum in vitro and in vivo, PLNs disassembled before entering tumors, which could explain the differences in their extravasation efficiency. These findings offer an opportunity to improve therapeutic cargo delivery to invasive GBM.

[*]co-corresponding authors.
[#]equal contribution

INTRODUCTION

Glioblastoma (GBM) is the most aggressive and predominant type of glioma in adults, with a historical survival of only 20 months [1, 2]. Although GBM generally does not metastasize to other organs, it displays a highly invasive phenotype by which glioma cells migrate in the brain away from the primary tumor mass, often along myelinated nerve tracks and blood vessels [3, 4]. Despite advances in the understanding of glioma biology, most novel therapies result in only a modest increase in patient survival and the inevitable progression of the disease [5]. Radiation therapy, the backbone of glioma therapy, leads to vascular damage and increased tumor permeability. However, it also increases invasiveness [6, 7]. The current therapies' main limitation is poor drug penetration across the blood-brain and blood-tumor barriers (BBTB) and insufficient drug delivery to glioma cells invading surrounding brain tissue [8–12]. While tumor progression leads to BBTB structural changes in neuronal death, astrocyte end-feet displacement, and heterogeneous pericyte subpopulations, the accumulation of drugs in brain tumors remains heterogeneous [12, 13]. Several strategies have been explored to improve delivery, including convection-enhanced delivery and focused ultrasound [14, 15]. However, these strategies have shown mixed results in the clinic and often require complex invasive procedures.

Nanoparticles and liposomes have recently been suggested as attractive solutions to improve the penetration of drugs to gliomas, with various chemistries, nanoparticle types, and targeting ligands being tested for improving trafficking across BBTB [5]. However, despite this gain in therapeutic efficacy through engineering [16], including targeting endothelial transporters [17–21], nanoparticle delivery systems still show heterogenous penetration, diffusion, and retention [22, 23]. Therefore, there is a desperate need for new delivery modalities across BBTB while emphasizing the targeting of the invasive edge of tumors.

Fluorescent indocarbocyanine lipids (**ICLs:** DiI, DiD, DiR) are popular choices for labeling and tracking cells and nanoparticles [24–27]. Besides being a valuable probe for tracking, ICLs could also be viewed as a model surrogate "payload" [28]. We have recently demonstrated that liposomal ICLs exhibit more efficient migration and retention in glioma and other solid tumors than liposomal fluorescent phospholipids [29]. Here, we report that a simple formulation of ICLs with DSPE-PEG2000 in PEGylated lipid nanoparticles (PLN) leads to their superior extravasation, migration, and retention in various glioma models following a single systemic injection. This phenomenon can be exploited to understand the delivery process and to improve imaging and drug delivery efficiency in GBM.

RESULTS

1. ICLs formulated in PEGylated lipid nanoparticles show better tumor penetration than liposomes and dextran

We formulated ICL (DiD) at 33 mol % with DSPE-PEG2000 into PEGylated lipid nanoparticles (PLNs, Fig. 1A, bottom). The addition of DSPE-PEG2000 was necessary since DiD alone is almost water-insoluble. For comparison, we prepared EPC/DSPE-PEG2000 liposomes with 0.4 mol % DiD (Fig. 1A, top). Liposomes had an average diameter of 125 nm, whereas PLNs were smaller, with an average diameter of 96 nm (Fig. 1A).

Both formulations appeared colloidally stable (Fig. 1B). At an equal molar concentration of DiD, the fluorescence of PLNs was about 90% lower than liposomes (Supplemental Fig. 1), likely due to quenching of their dye molecules being closely packed in PLNs. Using a high magnification confocal imaging, we show that both liposomes and PLNs are sub-micron-sized nanoparticles, with PLNs being more heterogeneous and less defined in shape than liposomes (Fig. 1C). To compare the efficiency of uptake *in vitro*, we incubated liposomal DiD or PLN-formulated DiD (0.7 μM) with either Matrigel™-based spheroids derived from U-87MG glioma cells or with organoids derived from mouse GL261 tumors and patient-derived xenograft GBM6 glioma tumors. Unlike spheroids, tumor organoids better recapitulate the tumor stroma and immune microenvironment [30]. Using confocal imaging, we observed much better DiD penetration for the PLN group that for the liposome group at the same Z-depth (Fig. 1D). Indeed, previous data suggest limited penetration of liposomes into spheroids [31]. Whole spheroid/organoid imaging confirmed significantly higher DiD accumulation in the PLN group than in the liposome group for U-87MG spheroids and GL261- and GBM6-derived organoids (Fig. 1E–F, p-values<0.0001, 0.014, 0.003, respectively).

Liposomal or PLN-formulated DiD administered via i.v. route at 0.14 μmol/kg in C57BL/6 mice showed similar plasma half-lives of DiD (174 min and 165 min, respectively (Fig. 2A)). In order to compare the extravasation efficiency in tumors, particles were injected in GL261 glioma-bearing mice along with FITC-lectin and Hoechst to stain blood vessels and nuclei, respectively. Brains were excised 1h post-injection, snap-frozen, sectioned into 1-2 mm slices, and immediately imaged non-fixed with a confocal microscope. This technique enables wide-field imaging of nanoparticles in intact tissue without introducing fixation-induced autofluorescence and lipid migration artifacts, especially given the non-fixable nature of the lipids used in the study [29, 32]. Liposomal DiD exhibited enhanced binding to tumor blood vessels and initial extravasation and migration as both discrete particles and diffuse fluorescence (Fig. 2B, arrows). Conversely, PLN-formulated DiD displayed a pattern of diffuse fluorescence that spread over the entire tumor area (Fig. 2B). Line profile drawn across representative tumor blood vessels confirmed limited migration of liposomal DiD, and extensive migration of PLN-formulated DiD (Fig. 2C). The extravasation was much more widespread in the PLN-formulated DiD group compared to the liposomal DiD group in terms of the percentage of tumor total fluorescence area (Fig. 2D, top; 92% and 23%, respectively; p-value<0.0001) and the percentage of tumor extravascular fluorescence areas (Fig. 2D, bottom; 82% and 13%, respectively; p-value<0.0001).

At 48h post-injection, both liposomal and PLN-formulated ICLs exhibited spreading of intratumoral fluorescence. However, a significantly larger area was positive for PLN-formulated DiD than liposomal DiD (Fig. 3A–C; total area: 62% vs 35%; p-value<0.0001). Occasionally, we observed fluorescence-positive areas at a distance from the tumors, but these were much dimmer than the tumors (not shown). *Ex vivo* imaging of organs showed an accumulation of liposomal and PLN-formulated DiD in the liver, spleen, kidneys, lungs, and intestine (Fig. 3D–E). Notably, PLN-formulated DiD showed more brain tumor accumulation than liposomal DiD. In order to compare the extravasation of ICLs in the same tumor, 0.14 μmol/kg of PLN-formulated DiI (DSPE-PEG2000/DiI 2:1; 87nm, Supplemental Fig. 2) and 0.14 μmol/kg of liposomal DiD (same formulation as above) were

co-injected in GL261 bearing mice. Confocal microscopy of fresh brain slices 48h post-injection confirmed significantly better migration and spreading for PLN-formulated DiI than liposomal DiD (Fig. 3F–G; *p*-value<0.0001). To account for the potential quenching of the dye in PLNs, we extracted ICLs with organic solvent from liver, kidney, spleen, and brain homogenates and quantified the amount of the lipid using the calibration curve prepared in the extracts of the respective organs (Supplemental Fig. 3), as described by us before [29]. The analysis showed higher accumulation (reported as percent of injected dose per gram tissue %ID/g) of PLN-formulated DiI than liposomal DiD in the liver and brain, but lower accumulation in kidneys and spleen (Fig. 3H). Whole-brain accumulation (Fig. 3I) was significantly higher for PLN-formulated DiI than for liposomal DiD (4.4%ID/g *vs.* 2.7%ID/g; Fig. 3I; *p*-value 0.04). While the exact weight of the intracranially implanted GL261 tumors could not be determined precisely, the brain's weight with a tumor is 15-20% more than a healthy brain. Therefore, the accumulation of PLN-formulated ICLs could be as much as 30% ID/g tumor, albeit this is an estimation.

Macromolecules, such as dextrans, accumulate in tumors and gliomas via the enhanced permeability and retention (EPR) effect [33, 34]. In order to compare tumor extravasation and accumulation of PLNs and dextran, we co-injected PLN-formulated DiD and 70kDa rhodamine-dextran in GL261 tumor-bearing mice. To compensate for the difference of the extinction coefficients between DiD (260,000 $M^{-1}cm^{-1}$) and rhodamine (106,000 $M^{-1}cm^{-1}$), we injected 0.14 μmol DiD/kg and 0.33 μmol rhodamine/kg. PLN-formulated DiD showed widespread diffuse extravasation at 1h, whereas the tumor extravasation of dextran was heterogeneous and focal (Fig. 4A–B). Furthermore, the rhodamine-positive area was significantly smaller than the DiD-positive area (Fig. 4B, *p*-value<0.0001). Also, there was no detectable rhodamine-dextran signal in tumors 48h post-injection (Fig. 4C–D), suggesting that tumor retention of PLN-formulated ICLs is also more efficient than that of macromolecular dextran.

2. PLN-formulated ICLs target immunosuppressive microenvironment and invasive tumor cells more efficiently than liposomal ICLs.

To compare the uptake of liposomal and PLN-formulated ICLs by cell types in tumors, we performed flow cytometry analysis at 48h post-injection of liposomal and PLN-formulated DiD in GL261 bearing mice (Fig. 5A; gating strategy described in Supplemental Fig. 4–6). The analysis showed that 65% of CD45− cells (tumor cells as well as other non-immune cells including endothelial cells and astrocytes) were DiD+ in the PLN group, *versus* only 4% in the liposome group (Fig. 5B, *p*-value 0.001), and 79% of lymphocytes were DiD+ in the PLN group, *versus* 19% in the liposome group (Fig. 5B, *p*-value<0.0001). Furthermore, 97% of myeloid cells were DiD+ in the PLN group, *versus* 61% DiD+ in the liposome group (Fig. 5B, *p*-value 0.014). Percentages of DiD+ cells in dendritic cells (DC), monocytic (mo) MDSCs, polymorphonuclear (PMN) MDSCs, and tumor-associated macrophages (TAMs) were over 70% in both groups (Fig. 5C). The percentage of DiD+ DCs was significantly higher in the PLN group (Fig. 5C, *p*-value 0.016). The uptake efficiency, measured as the mean fluorescence intensity (MFI), revealed significantly higher uptake in the PLN group than in the liposomal group for DCs, PMN MDSCs, and TAMs (Fig. 5D, *p*-values 0.006, 0.002, and 0.003, respectively). Lymphoid cells showed significantly higher percentage of

DiD+ B-cells, Tregs (CD4+CD25+), CD4+ and CD8+ T cells, and NK cells in the PLN group compared to the liposomal group (Fig. 5E, *p*-values 0.0004, 0.005, 0.0001, 0.0003, 0.035, respectively). Lymphoid cells showed a significantly increased MFI in CD4+CD25+ Tregs in the PLN group compared to the liposomal group (Fig. 5F, *p*-values<0.0001, 0.003, respectively). Thus, these results suggest that the lipid formulation determines the uptake efficiency by the tumor microenvironment, and PLNs accumulate in immunosuppressive cells more efficiently than liposomes.

While many publications focused on improving the total delivery of nanoparticles to gliomas [5], to our best knowledge, the delivery to the glioma margin and invasive cells has not been studied in detail. Therefore, we examined the accumulation of PLN-formulated ICLs at the tumor/brain interface in several intracranial models. Forty-eight hours post-co-injection of 0.14 μmol/kg of PLN-formulated DiI and liposomal DiD, much greater labeling of the margin was seen with DiI compared to DiD in the GL261 bearing mice (Fig. 6A, arrows). PEGylated liposomal doxorubicin (aka Doxil®) is the clinically approved fluorescent liposome that often serves a “benchmark” for comparison with other nano delivery systems [35]. Notably, Doxil showed limited clinical efficacy in gliomas [36]. Therefore, we coinjected generic Doxil (LipoDox®) and DiD PLN in the GL261 glioma-bearing mice to compare delivery to the invasive margin. Due to differences in fluorescence properties (DOX ε=10,400 $M^{-1}cm^{-1}$ and DiD ε=260,000 $M^{-1}cm^{-1}$), we injected 90-fold molar excess of DOX over DiD and also adjusted the gain of the microscope by imaging the DOX:DiD mix spiked in tumor homogenate to account for any variability in fluorophore signal in tumor (Supplemental Fig. 7 and Methods). Confocal microscopy of fresh brain slices 48h post-injection revealed a significant difference in intratumoral distribution between DiD and DOX (Fig. 6B, top row). Notably, DiD accumulated in the entire tumor, including the margin, whereas DOX localization was confined to perivascular areas.

Since GL261 is not an invasive tumor, we studied the distribution of PLN-formulated DiD and DOX in highly invasive genetically engineered mouse models (GEMM) of supratentorial high-grade and diffuse midline glioma [37]. In GEMMs, similarly to the GL261 model, there was an extensive spreading and localization of DiD in the center and edge of the tumor, with DiD localization within breakaway islands of tumor cells (Fig. 6B, middle and bottom row). The accumulation of DOX was again restricted to the perivascular areas. In order to localize DiD in the margin, tumors were stained for engineered human IL13 receptor alpha 2 (IL13Rα2) on the surface of the cancer cells. In addition, the tumor’s margin was visualized with an H&E stain on sequential tissue sections. This allowed us to determine a colocalization of DiD with the tumor margin and with brain-invading tumor cells. According to Fig. 7A–B, several breakaway IL13Rα2+ cells could be observed near the margin, and these cells were also positive for DiD.

3. PLNs undergo disassembly in vivo, which could explain better tumor penetration efficiency than liposomes.

A recent paper hypothesized that DSPE-PEG2000-based lipid nanodiscs have higher malleability than liposomes, which might facilitate their squeezing through pores in the vasculature [38]. To test if this is the case with PLNs, we compared the filterability of

liposomes and PLNs through 0.1μm pore size filters, which is on the order of the gaps observed in the tumor endothelium [39–42]. Supplemental Fig. 8 shows that both liposomes and PLNs almost entirely pass through 0.1μm pore membrane, suggesting that both types of particles are malleable enough to make through the vascular pores. We, therefore, hypothesized that changes to the formulations taking place in serum could explain the penetration efficiency. Therefore, we prepared PLNs and liposomes labeled with DiI only, or with both DiI and DiD. In the latter case, the proximity of the dyes should lead to fluorescence resonance energy transfer (FRET) between the Cy3 headgroup of DiI (donor) and the Cy5 headgroup of DiD (acceptor), leading to a quenching of DiI fluorescence as compared to DiI only particles. Indeed, PLNs exhibited almost complete FRET efficiency of 0.97, whereas liposomes exhibited lower but still significant FRET efficiency of 0.38 (Supplemental Fig. 9). Addition of serum led to an immediate unqenching and ~60% relative loss of FRET in PLNs (Fig. 8A and Supplemental Fig. 9). In contrast, the addition of serum did not decrease, but instead increased FRET efficiency in liposomes (Fig. 8A and Supplemental Fig. 9), suggesting compaction of lipids in the bilayer, or other effects of the protein corona on fluorophores.

Previously, we used confocal imaging of double-labeled liposomes and demonstrated their stability in plasma after injection in mice [29, 32]. To compare the integrity of PLNs and liposomes, we injected DiI/DiD-labeled PLNs and liposomes in mice and collected plasma 15 min post-injection. According to high magnification confocal images (Fig. 8B), liposomes were intact and showed colocalization of DiI and DiD before and after the injection. At the same time, PLNs showed some colocalization before injection, but a lack of colocalization after the injection, with both dyes appearing to be separated. The resolution of confocal microscopy is not sufficient to determine if PLNs separated into individual lipids or smaller nanoparticles. Finally, we correlated the observed disintegration of PLNs *in vivo* with very early steps of tumor entry. DiI/DiD PLNs or DiI/DiD liposomes were injected in GL261 glioma-bearing mice, and extracted brains were snap-frozen at 15 min post-injection, cryosectioned, and immediately imaged with high-magnification confocal microscopy (Fig. 8C–D). Liposomes showed primarily binding to blood vessels and high degree of colocalization of DiI and DiD. On the other hand, PLN-injected mice showed spreading of DiI and DiD away from the endothelium and much lower colocalization of DiI and DiD outside of blood vessels, suggesting that the dyes enter tumors separated (Fig. 8C–D).

DISCUSSION

Due to the heterogeneous permeability and presence of efflux transporters in the BBTB [41], there is a dire need to improve drug delivery to glioma [43]. Liposomes, lipid nanoparticles, and lipid-drug conjugates are some of the most promising candidates for cancer delivery [43–46]. We demonstrated highly efficient extravasation, and penetration of ICLs formulated in a simple nanoformulation without decoration with transcytosis ligands (e.g., glucose transporter substrates or growth factors) or use of physical methods such as convection-enhanced delivery and focused ultrasound in glioma tumors. Moreover, while several classes of nanoparticles can achieve an improved degree of BBTB penetration [16], targeting the invasive cells, a major problem in GBM, remains unsolved [5]. Importantly,

our study demonstrated the fluorescent lipid delivery to the invasive edge in aggressive models of supratentorial high-grade and diffuse midline glioma in the immunocompetent host. Furthermore, in addition to the invasive cells, PLN-formulated ICLs showed a better delivery than liposome-formulated ICLs to the tumor's immunosuppressive myeloid cells. Based on our data, the next logical step is to use PLN-formulated ICLs as carriers for drugs for enhanced delivery of brain-impermeable small molecules, e.g., by conjugating drugs *via* cleavable self-immolating linkers [46].

The efficient and specific tumor extravasation and penetration of PLNs are contrary to the prevailing dogma in the drug delivery field that serum stability is one of the prerequisites for successful nanoparticle design. However, the success of serum-unstable nanoparticle nab-paclitaxel (Abraxane®) provides an argument against this dogma, and that other factors besides serum stability dictate nanomedicine performance. While the estimated number of injected liposomal particles was higher than PLN particles (at the same ICL dose), the disintegration of PLNs into smaller structures after injection could explain the facilitated entry and migration of ICLs in tumors. While there is evidence of endothelial pores/gaps in tumors including gliomas in previous studies [40–42], superior extravasation of ICLs to 70kDa dextran suggests a more complex mechanism than simple diffusion via gaps. Several recent papers suggested transcytosis as the primary mechanism of tumor accumulation of nanocarriers [47–50]. ICLs are known to efficiently label extracellular vesicles (EVs), including exosomes [51, 52]. Due to the efficient lateral diffusion in membranes [53–55], ICLs could become incorporated into the transcytosis machinery of endothelial or tumor cells. A high affinity of ICLs to cells could also explain the efficient retention of therse lipids in tumors. Understanding the mechanisms of extravasation, distribution, and retention of ICLs requires further investigation using a combination of relevant knockdowns in animal models and specific inhibitors of endocytosis and transcytosis. Such studies will be essential for understanding and improving cancer nanomedicine performance.

MATERIALS AND METHODS

Materials:

DiD (1,1'-Dioctadecyl-3,3,3',3'-Tetramethylindotricarbocyanine, 4-chlorobenzenesulfonate salt), and DiI (1,1'-Dioctadecyl-3,3,3',3'-Tetramethylindotricarbocyanine Perchlorate) were from Biotium (Hayward, CA, USA) and were stored as 10 mM sock in ethanol. Whatman Nucleopore Track-Etch Membranes, bovine serum albumin, and the chemicals for synthesis were from Sigma-Aldrich (St. Louis, MO, USA). Nitrocellulose membrane (0.45 μm) was from Bio-Rad (Hercules, CA, USA). Egg phosphatidylcholine (EPC), distearoyl phosphatidylethanolamine (DSPE)-PEG2000 were from Avanti Polar Lipids (Alabaster, AL, USA). Nuclear staining reagent Hoechst 33342 trihydrochloride trihydrate was purchased from Life Technologies (Carlsbad, CA, USA). Fetal bovine calf serum, RPMI 1640 growth medium supplemented with L-glutamine were from Corning Inc. (New York, NY, USA). FITC-labeled tomato lectin (FL-1171-1) was from Vector Laboratories (Burlingame, CA, USA). PEGylated liposomal doxorubicin (LipoDox®, Sun Pharma) was obtained in sterile leftover vials from the University of Colorado Cancer Center pharmacy. Rhodamine B dextran (70kDa) was from ThermoFisher.

Liposome and PLN preparation:

Lipids were mixed at the following molar ratios: EPC/DSPE-PEG2000/DiD (mole %: 95/5/0.4) in chloroform and dried under a nitrogen stream. The dry lipid cake was resuspended in PBS for a total DiD concentration of 35μM, then incubated at 37°C for 30 minutes. The solution was extruded using a syringe extruder (Avestin, Ottawa, Canada) through Whatman Nucleopore Track-Etch Membranes (100 nm pore size 15 times). To prepare PLNs, DiI or DiD was mixed with DSPE-PEG2000 at 1:2 mole ratio in ethanol, dried, and resuspended in PBS at 35μM DiD. NanoSight 300 (Malvern, UK) was used to measure the size of the particles. Liposomes and PLNs were stored at 4°C for a maximum period of 4 weeks.

Cell culture:

GL261 cells were obtained from the National Cancer Institute (NCI) and were grown at 37°C in RPMI 1640 medium containing 10% heat-inactivated fetal bovine serum, 10 mM HEPES, 100 U/ml penicillin, and 100 ng/ml streptomycin (all from Corning Inc. New York, NY, USA). U-87MG cells were from American Tissue Culture Collection and were grown in DMEM medium with 4.5g/l glucose and L-glutamine without sodium pyruvate. The medium was supplemented with 10% heat-inactivated fetal bovine serum, 100 U/ml penicillin, and 100 ng/ml streptomycin.

To generate spheroids from glioma cells, adherent U-87MG cells were enzymatically lifted with trypsin-EDTA, pelleted by centrifugation, counted, and resuspended in NeuroCult™ NS-A Basal Medium with human recombinant epidermal growth factor (20ng/ml), basal fibroblast growth factor (10 ng/ml), heparin solution (2 ng/ml) (all from StemCell Technologies, Vancouver, Canada), and StemPro™ neural supplement (1% v/v, Thermo Fischer) to a concentration of 2000 cells/μl. The cell suspension was mixed with cold Matrigel® (Corning, Tewksbury, MA) at a 1:4 ratio. The Matrigel-cell suspension was added to the indentations created in the parafilm molds (20 μl) and polymerized for one hour at 37°C. After one hour, the spheroids were manually dislodged from the parafilm molds into DMEM and cultured for 72 hours at standard conditions (37°C, 5% CO2, 95% humidity). After 72 hours, the spheroids were placed on an orbital shaker within an incubator, where they remained for 11 additional days. On day 14, the Matrigel was removed using Cell Recovery Solution (Corning) per the manufacturer's protocol. Briefly, spheroids were washed with cold PBS and gently resuspended in 1 ml of cold Cell Recovery Solution for 5 min. After 5 min, spheroids were washed with cold PBS three additional times and placed back into DMEM for seven days. After 21 days of culture, spheroids were ready for experimental use.

Tumor organoids were generated from GBM6 and GL261 orthotopic tumors as previously described [56]. Briefly, GBM6 and GL261 were implanted intracranially in NSG and C57BL/6 mice, respectively. Following tumor engraftment and development, mice were sacrificed, and tumors were dissected from brains. Tumors were subsequently diced into approximately 0.5 mm^3 fragments with a sterile blade, washed twice with PBS, and cultured in DMEM supplemented with 10% FBS on an orbital shaker within a tissue culture incubator. After 72 hours of culture, tumor explants were ready for experimental use.

Animal experiments:

The University of Colorado and Northwestern University Institutional Animal Care and Use Committees (IACUC) approved animal experiments (protocols 103913(11) and IS00002999, respectively). For circulation half-life, healthy C57BL/6 mice (6-8 weeks old females) were injected with PLNs or liposomes (0.14μmol/kg of ICL). Blood was collected *via* periorbital plexus using heparin glass capillaries, and the plasma was separated by centrifugation at 500 *g* for 5 min. For brain tumors, C57BL/6 mice (6-8 weeks old) were implanted with a total of $4x10^5$ GL261 cells per animal using an established protocol.[57] NSG mice were implanted with $2x10^5$ GBM6 cells as previously described [58]. For supratentorial high-grade and diffuse midline glioma models [37], nestin-*tva* (NTV-a) $p53^{fl/fl}$ mice were injected with RCAS-PDGFB/IL13Ra2 and RCAS-Cre DF-1 avian virus producer cells to form tumors that express invasive brain tumor marker human IL13Rα2 [59, 60]. Experiments were performed when tumors were fully developed in each model. Mice were injected i.v with 80-100 μl boluses. Next, mice were preinjected 1h before sacrificing with 50 μl of FITC-tomato lectin (1 mg/ml) and 50 μl Hochest33324 (2 mg/ml) to visualize the vasculature and the nuclei, respectively. Mice were sacrificed at different times post injection with carbon dioxide, followed by cardiac perfusion with PBS through the left ventricle.

Organ and plasma imaging:

The organs were excised and scanned with a Bio-Rad camera imager equipped with a Cy5 filter for DiD detection or Li-COR Odyssey for Cy7 detection. Mean fluorescence was determined from 8-bit TIFF images using Fiji software by subtracting the background, drawing a region of interest around the organs or tumors, and using the “Measure” function to determine mean gray values. Such measurement is independent of the organ cross-section area and is roughly proportional to the dye concentration. The mean gray values of non-injected organs and tumors were subtracted from the measurements and plotted with Prism version 8.3.0 software (GraphPad, San Diego, CA). For fluorescence clearance, plasma was dotted on a nitrocellulose membrane, scanned as above. The mean fluorescence of dots was plotted versus time using Prism and fitted into mono-exponential decay to calculate half-life.

Microscopy and image quantification:

Nikon Eclipse AR1HD inverted confocal microscope with 405 nm (Hoechst), 488 nm (FITC), 561 nm (DiI), and 640 nm (DiD) excitation lasers and corresponding emission filters was used. For high magnification imaging of liposomes and nanoparticles, particle solution was diluted at 1:1000 before injection. Plasma collected after injection was diluted at 1:100 in PBS. The diluted samples were mixed with glycerol at 1:1 ratio, and 2 μl were placed on a slide and covered with a glass coverslip. The preparations were imaged under Apo60 objective at 2048 x 2048 resolution. For intact tumor slice imaging, mice were perfused via cardiac perfusion with PBS, brains were snap-frozen on dry ice for whole tumor imaging and sliced with a blade in 1-2mm thick slices. The slices were placed on a glass slide and immediately imaged using Plan Apo 10 or Plan Apo 20 objectives. Each tumor was imaged within 30 min to avoid artifacts. For cryosections in Fig. 7–8, brains were snap-frozen, cryo-sectioned in 7μm sections, fixed with formalin for 10 min and imaged under 20x objective. Multiple random image areas were acquired per section at 512x512

or 1024x1024 resolution. Images were quantified with FIJI using built-in or customized macros. Briefly, for fluorescent area quantification, 8-bit gray image stacks were manually thresholded, and the percentages of binary (positive) areas in the green and red channels were calculated using the “Measure” function. For calculation of the percentage of an area outside of lectin-positive blood vessels, the lectin staining was selected in the FITC channel, applied to all channels, and the dye-positive area outside the selections was thresholded and calculated as described above. For fluorescence profile, a perpendicular line was drawn outwards from the periphery of blood vessels, and the “Plot Profile” function was used to determine pixel values versus distance. All the data were plotted with Prism.

ICL quantification:

ICLs were extracted using a modified Bligh-Dyer method [61]. Briefly, 50-100 mg pieces of wet liver tissue (mid lobe), or whole spleen, kidney, and brain of tumor mice were homogenized as described previously [29]. Ten parts of chloroform/methanol (2:1) were added, and the samples were mixed at 1400 rpm for 2 h at room temperature. The tubes were centrifuged at 500 g for 10 min. The organic phase (bottom, approximately 80% of the added amount was recovered) was carefully collected, dotted as 2 μl aliquots on a PVDF membrane (Millipore), and scanned for ICL fluorescence with a Bio-Rad imager as described above. Two-fold dilutions of ICLs in extracts of organs and tumor-bearing brains from non-injected mice were dotted on the same membrane and scanned together with the samples. The calibration curves are in supplemental Fig. 3. The percent of the injected dose in the extracts was calculated and divided by the respective wet tissue weight.

Immunostaining and flow cytometry:

For immunostaining, mice with supratentorial high-grade or diffuse midline glioma tumors [62] were injected with DiD liposomes and perfused 48 h post-injection. Brains were snap-frozen in OCT in liquid nitrogen and immediately sectioned with a cryostat into 7 μm sections. The sections were fixed for 10 min with 4% formalin, blocked with 10% goat serum, and stained with mouse anti-human IL13Rα2 antibody (clone 47, BioLegend) and goat anti-mouse Alexa Fluor™ Plus 555 secondary antibody (ThermoFisher).

A single-cell suspension of brain tissue was prepared for flow cytometry analysis as previously described [57]. The markers, including for tumor associated macrophages and myeloid cell populations were based on previous publications [57, 63, 64]. Single-cell isolates were pre-blocked with Ultra-LEAF purified anti-mouse CD16/32 antibody (BioLegend, San Diego, CA) in PBS supplemented with 2% FBS 10 min at 4 °C before antibody staining. The following flow cytometry panel (BioLegend) was used for cell staining: anti-CD4-FITC, anti-CD8-BV605, or -PE-Cy7, anti-CD19-BV711, anti-CD25-PE, anti-NK1.1-PE-Cy7, anti-Ly6G-FITC, anti-CD11b-Pacific Blue, anti-CD11c-BV605, anti-Ly6C-AlexaFluor 700, anti-F4/80-PE, all at a 1:200 dilution. Cells were counterstained with fixable *via*bility dye eFluor 780 (Invitrogen) to exclude dead cells from analysis. After incubation on ice for 20 minutes and washing, cells were analyzed for surface staining using the BD FACSymphony flow cytometer (Becton Dickinson, Franklin Lakes, NJ) and FlowJo software Version 10.6 (FlowJo, LLC).

FRET assay:

PLNs and liposomes were prepared with DiI only, DiD only, or DiI/DiD as described above. Particles were added at 2μM dye to PBS or to 40% mouse serum at 37°C in a transparent bottom microwell plate, and fluorescence of DiI (donor) was measured at 550 nm excitation/570 nm emission for 1h using Spectramax M2 fluorescence microplate reader. FRET efficiency in PBS and in serum was calculated according to the formula:

$$1 - \frac{I_{DiI-DiD}}{I_{DiI}},$$

Where $I_{DiI\text{-}DiI}$ is the fluorescence intensity of double-labeled particles, and I_{DiI} is the fluorescence intensity of single-labeled particles. The efficiency was then plotted as is or as the percentage of the initial efficiency (before serum).

Supplementary Material

Refer to Web version on PubMed Central for supplementary material.

ACKNOWLEDGMENTS

The study was supported by the National Institutes of Health (NIH) grants R01CA257958-01A1 to D.S. and I.V.B and R01NS122395 and R01NS106379 to I.V.B.

REFERENCES

[1]. Stupp R, Taillibert S, Kanner A, Read W, Steinberg D, Lhermitte B, Toms S, Idbaih A, Ahluwalia MS, Fink K, Di Meco F, Lieberman F, Zhu JJ, Stragliotto G, Tran D, Brem S, Hottinger A, Kirson ED, Lavy-Shahaf G, Weinberg U, Kim CY, Paek SH, Nicholas G, Bruna J, Hirte H, Weller M, Palti Y, Hegi ME, Ram Z, Effect of Tumor-Treating Fields Plus Maintenance Temozolomide vs Maintenance Temozolomide Alone on Survival in Patients With Glioblastoma: A Randomized Clinical Trial, JAMA, 318 (2017) 2306–2316. [PubMed: 29260225]

[2]. Hottinger AF, Pacheco P, Stupp R, Tumor treating fields: a novel treatment modality and its use in brain tumors, Neuro Oncol, 18 (2016) 1338–1349. [PubMed: 27664860]

[3]. Giese A, Westphal M, Glioma invasion in the central nervous system, Neurosurgery, 39 (1996) 235–250; discussion 250-232. [PubMed: 8832660]

[4]. Paw I, Carpenter RC, Watabe K, Debinski W, Lo HW, Mechanisms regulating glioma invasion, Cancer Lett, 362 (2015) 1–7. [PubMed: 25796440]

[5]. Shergalis A, Bankhead A 3rd, Luesakul U, Muangsin N, Neamati N, Current Challenges and Opportunities in Treating Glioblastoma, Pharmacol Rev, 70 (2018) 412–445. [PubMed: 29669750]

[6]. Birch J, Gilmour L, Strathdee K, Vallatos A, McKinnon H, Drysdale M, Olson M, Chalmers A, Irradiation of glioblastoma cells can promote enhanced motility and invasiveness, both in vitro and in vivo through activation of MRCK, Neuro-Oncology, 20 (2018) i3-i3.

[7]. Park HJ, Griffin RJ, Hui S, Levitt SH, Song CW, Radiation-induced vascular damage in tumors: implications of vascular damage in ablative hypofractionated radiotherapy (SBRT and SRS), Radiat Res, 177 (2012) 311–327. [PubMed: 22229487]

[8]. Krenciute G, Prinzing BL, Yi Z, Wu MF, Liu H, Dotti G, Balyasnikova IV, Gottschalk S, Transgenic Expression of IL15 Improves Antiglioma Activity of IL13Ralpha2-CAR T Cells but Results in Antigen Loss Variants, Cancer Immunol Res, 5 (2017) 571–581. [PubMed: 28550091]

[9]. Pardridge WM, The blood-brain barrier: bottleneck in brain drug development, NeuroRx, 2 (2005) 3–14. [PubMed: 15717053]

[10]. Pitz MW, Desai A, Grossman SA, Blakeley JO, Tissue concentration of systemically administered antineoplastic agents in human brain tumors, J Neurooncol, 104 (2011) 629–638. [PubMed: 21400119]

[11]. Lockman PR, Mittapalli RK, Taskar KS, Rudraraju V, Gril B, Bohn KA, Adkins CE, Roberts A, Thorsheim HR, Gaasch JA, Huang S, Palmieri D, Steeg PS, Smith QR, Heterogeneous blood-tumor barrier permeability determines drug efficacy in experimental brain metastases of breast cancer, Clin Cancer Res, 16 (2010) 5664–5678. [PubMed: 20829328]

[12]. Sarkaria JN, Hu LS, Parney IF, Pafundi DH, Brinkmann DH, Laack NN, Giannini C, Burns TC, Kizilbash SH, Laramy JK, Swanson KR, Kaufmann TJ, Brown PD, Agar NYR, Galanis E, Buckner JC, Elmquist WF, Is the blood-brain barrier really disrupted in all glioblastomas? A critical assessment of existing clinical data, Neuro Oncol, 20 (2018) 184–191. [PubMed: 29016900]

[13]. Arvanitis CD, Ferraro GB, Jain RK, The blood-brain barrier and blood-tumour barrier in brain tumours and metastases, Nat Rev Cancer, 20 (2020) 26–41. [PubMed: 31601988]

[14]. Jahangiri A, Chin AT, Flanigan PM, Chen R, Bankiewicz K, Aghi MK, Convection-enhanced delivery in glioblastoma: a review of preclinical and clinical studies, J Neurosurg, 126 (2017) 191–200. [PubMed: 27035164]

[15]. Arvanitis CD, Askoxylakis V, Guo Y, Datta M, Kloepper J, Ferraro GB, Bernabeu MO, Fukumura D, McDannold N, Jain RK, Mechanisms of enhanced drug delivery in brain metastases with focused ultrasound-induced blood-tumor barrier disruption, Proc Natl Acad Sci U S A, 115 (2018) E8717–E8726. [PubMed: 30150398]

[16]. Tang W, Fan W, Lau J, Deng L, Shen Z, Chen X, Emerging blood-brain-barrier-crossing nanotechnology for brain cancer theranostics, Chem Soc Rev, 48 (2019) 2967–3014. [PubMed: 31089607]

[17]. Wang X, Zhang Q, Lv L, Fu J, Jiang Y, Xin H, Yao Q, Glioma and microenvironment dual targeted nanocarrier for improved antiglioblastoma efficacy, Drug Deliv, 24 (2017) 1401–1409. [PubMed: 28933201]

[18]. Huang Y, Liu W, Gao F, Fang X, Chen Y, c(RGDyK)-decorated Pluronic micelles for enhanced doxorubicin and paclitaxel delivery to brain glioma, Int J Nanomedicine, 11 (2016) 1629–1641. [PubMed: 27143884]

[19]. Sun Z, Zhang Y, Cao D, Wang X, Yan X, Li H, Huang L, Qu X, Kong C, Qin H, Wang M, Xu W, Liang L, PD-1/PD-L1 pathway and angiogenesis dual recognizable nanoparticles for enhancing chemotherapy of malignant cancer, Drug Deliv, 25 (2018) 1746–1755. [PubMed: 30394118]

[20]. Passarella RJ, Spratt DE, van der Ende AE, Phillips JG, Wu H, Sathiyakumar V, Zhou L, Hallahan DE, Harth E, Diaz R, Targeted nanoparticles that deliver a sustained, specific release of Paclitaxel to irradiated tumors, Cancer Res, 70 (2010) 4550–4559. [PubMed: 20484031]

[21]. Wu H, Lu H, Xiao W, Yang J, Du H, Shen Y, Qu H, Jia B, Manna SK, Ramachandran M, Xue X, Ma Z, Xu X, Wang Z, He Y, Lam KS, Zawadzki RJ, Li Y, Lin TY, Sequential Targeting in Crosslinking Nanotheranostics for Tackling the Multibarriers of Brain Tumors, Adv Mater, 32 (2020) e1903759. [PubMed: 32078198]

[22]. Grodzinski P, Farrell D, Future opportunities in cancer nanotechnology--NCI strategic workshop report, Cancer Res, 74 (2014) 1307–1310. [PubMed: 24413533]

[23]. Hull LC, Farrell D, Grodzinski P, Highlights of recent developments and trends in cancer nanotechnology research--view from NCI Alliance for Nanotechnology in Cancer, Biotechnol Adv, 32 (2014) 666–678. [PubMed: 23948249]

[24]. Progatzky F, Dallman MJ, Lo Celso C, From seeing to believing: labelling strategies for in vivo cell-tracking experiments, Interface Focus, 3 (2013) 20130001. [PubMed: 23853708]

[25]. Zagorodnyuk VP, Kyloh M, Nicholas S, Peiris H, Brookes SJ, Chen BN, Spencer NJ, Loss of visceral pain following colorectal distension in an endothelin-3 deficient mouse model of Hirschsprung's disease, J Physiol, 589 (2011) 1691–1706. [PubMed: 21320883]

[26]. Kalchenko V, Shivtiel S, Malina V, Lapid K, Haramati S, Lapidot T, Brill A, Harmelin A, Use of lipophilic near-infrared dye in whole-body optical imaging of hematopoietic cell homing, J Biomed Opt, 11 (2006) 050507. [PubMed: 17092148]

[27]. Lo Celso C, Fleming HE, Wu JW, Zhao CX, Miake-Lye S, Fujisaki J, Cote D, Rowe DW, Lin CP, Scadden DT, Live-animal tracking of individual haematopoietic stem/progenitor cells in their niche, Nature, 457 (2009) 92–96. [PubMed: 19052546]

[28]. Yang C, Chen F, Ren P, Lofchy L, Wan C, Shen J, Wang G, Gaikwad H, Ponder J, Jordan CT, Scheinman R, Simberg D, Delivery of a model lipophilic membrane cargo to bone marrow via cell-derived microparticles, Journal of controlled release : official journal of the Controlled Release Society, 326 (2020) 324–334. [PubMed: 32682903]

[29]. Wang G, Zannikou M, Lofchy L, Li Y, Gaikwad H, Balyasnikova IV, Simberg D, Liposomal Extravasation and Accumulation in Tumors as Studied by Fluorescence Microscopy and Imaging Depend on the Fluorescent Label, ACS nano, (2021).

[30]. Rybin MJ, Ivan ME, Ayad NG, Zeier Z, Organoid Models of Glioblastoma and Their Role in Drug Discovery, Front Cell Neurosci, 15 (2021) 605255. [PubMed: 33613198]

[31]. Niora M, Pedersbaek D, Munter R, Weywadt MFV, Farhangibarooji Y, Andresen TL, Simonsen JB, Jauffred L, Head-to-Head Comparison of the Penetration Efficiency of Lipid-Based Nanoparticles into Tumor Spheroids, ACS Omega, 5 (2020) 21162–21171. [PubMed: 32875252]

[32]. Li Y, Lofchy L, Wang G, Gaikwad H, Fujita M, Simberg D, PEGylated Liposomes Accumulate in the Areas Relevant to Skin Toxicities via Passive Extravasation across “Leaky” Endothelium, ACS nano, (2022).

[33]. Matsumura Y, Maeda H, A new concept for macromolecular therapeutics in cancer chemotherapy: mechanism of tumoritropic accumulation of proteins and the antitumor agent smancs, Cancer Res, 46 (1986) 6387–6392. [PubMed: 2946403]

[34]. Natarajan R, Northrop N, Yamamoto B, Fluorescein Isothiocyanate (FITC)-Dextran Extravasation as a Measure of Blood-Brain Barrier Permeability, Curr Protoc Neurosci, 79 (2017) 9 58 51–59 58 15.

[35]. Sun D, Zhou S, Gao W, What Went Wrong with Anticancer Nanomedicine Design and How to Make It Right, ACS Nano, 14 (2020) 12281–12290. [PubMed: 33021091]

[36]. Ananda S, Nowak AK, Cher L, Dowling A, Brown C, Simes J, Rosenthal MA, Cooperative N-O Trials Group for, Phase 2 trial of temozolomide and pegylated liposomal doxorubicin in the treatment of patients with glioblastoma multiforme following concurrent radiotherapy and chemotherapy, J Clin Neurosci, 18 (2011) 1444–1448. [PubMed: 21813279]

[37]. Seblani M, Zannikou M, Duffy JT, Levine RN, Liu Q, Horbinski CM, Becher OJ, Balyasnikova IV, A New Mouse Model of Diffuse Midline Glioma to Test Targeted Immunotherapies, bioRxiv, (2021).

[38]. Dane EL, Belessiotis-Richards A, Backlund C, Wang J, Hidaka K, Milling LE, Bhagchandani S, Melo MB, Wu S, Li N, Donahue N, Ni K, Ma L, Okaniwa M, Stevens MM, Alexander-Katz A, Irvine DJ, STING agonist delivery by tumour-penetrating PEG-lipid nanodiscs primes robust anticancer immunity, Nat Mater, 21 (2022) 710–720. [PubMed: 35606429]

[39]. Hashizume H, Baluk P, Morikawa S, McLean JW, Thurston G, Roberge S, Jain RK, McDonald DM, Openings between defective endothelial cells explain tumor vessel leakiness, Am J Pathol, 156 (2000) 1363–1380. [PubMed: 10751361]

[40]. Monsky WL, Fukumura D, Gohongi T, Ancukiewcz M, Weich HA, Torchilin VP, Yuan F, Jain RK, Augmentation of transvascular transport of macromolecules and nanoparticles in tumors using vascular endothelial growth factor, Cancer Res., 59 (1999) 4129–4135. [PubMed: 10463618]

[41]. Belykh E, Shaffer KV, Lin C, Byvaltsev VA, Preul MC, Chen L, Blood-Brain Barrier, Blood-Brain Tumor Barrier, and Fluorescence-Guided Neurosurgical Oncology: Delivering Optical Labels to Brain Tumors, Front Oncol, 10 (2020) 739. [PubMed: 32582530]

[42]. Hobbs SK, Monsky WL, Yuan F, Roberts WG, Griffith L, Torchilin VP, Jain RK, Regulation of transport pathways in tumor vessels: role of tumor type and microenvironment, Proc Natl Acad Sci U S A, 95 (1998) 4607–4612. [PubMed: 9539785]

[43]. Golan T, Grenader T, Ohana P, Amitay Y, Shmeeda H, La-Beck NM, Tahover E, Berger R, Gabizon AA, Pegylated liposomal mitomycin C prodrug enhances tolerance of mitomycin C: a phase 1 study in advanced solid tumor patients, Cancer Med, 4 (2015) 1472–1483. [PubMed: 26172205]

[44]. Signorell RD, Luciani P, Brambilla D, Leroux JC, Pharmacokinetics of lipid-drug conjugates loaded into liposomes, Eur J Pharm Biopharm, 128 (2018) 188–199. [PubMed: 29678733]

[45]. Puri A, Loomis K, Smith B, Lee JH, Yavlovich A, Heldman E, Blumenthal R, Lipid-based nanoparticles as pharmaceutical drug carriers: from concepts to clinic, Crit Rev Ther Drug Carrier Syst, 26 (2009) 523–580. [PubMed: 20402623]

[46]. Irby D, Du C, Li F, Lipid-Drug Conjugate for Enhancing Drug Delivery, Mol Pharm, 14 (2017) 1325–1338. [PubMed: 28080053]

[47]. Thurston G, McLean JW, Rizen M, Baluk P, Haskell A, Murphy TJ, Hanahan D, McDonald DM, Cationic liposomes target angiogenic endothelial cells in tumors and chronic inflammation in mice, J Clin Invest, 101 (1998) 1401–1413. [PubMed: 9525983]

[48]. Liu X, Lin P, Perrett I, Lin J, Liao YP, Chang CH, Jiang J, Wu N, Donahue T, Wainberg Z, Nel AE, Meng H, Tumor-penetrating peptide enhances transcytosis of silicasome-based chemotherapy for pancreatic cancer, J Clin Invest, 127 (2017) 2007–2018. [PubMed: 28414297]

[49]. Sindhwani S, Syed AM, Ngai J, Kingston BR, Maiorino L, Rothschild J, MacMillan P, Zhang Y, Rajesh NU, Hoang T, Wu JLY, Wilhelm S, Zilman A, Gadde S, Sulaiman A, Ouyang B, Lin Z, Wang L, Egeblad M, Chan WCW, The entry of nanoparticles into solid tumours, Nat Mater, 19 (2020) 566–575. [PubMed: 31932672]

[50]. Liu Y, Huo Y, Yao L, Xu Y, Meng F, Li H, Sun K, Zhou G, Kohane DS, Tao K, Transcytosis of Nanomedicine for Tumor Penetration, Nano Lett, 19 (2019) 8010–8020. [PubMed: 31639306]

[51]. Grange C, Tapparo M, Bruno S, Chatterjee D, Quesenberry PJ, Tetta C, Camussi G, Biodistribution of mesenchymal stem cell-derived extracellular vesicles in a model of acute kidney injury monitored by optical imaging, Int J Mol Med, 33 (2014) 1055–1063. [PubMed: 24573178]

[52]. Morelli AE, Larregina AT, Shufesky WJ, Sullivan ML, Stolz DB, Papworth GD, Zahorchak AF, Logar AJ, Wang Z, Watkins SC, Falo LD Jr., Thomson AW, Endocytosis, intracellular sorting, and processing of exosomes by dendritic cells, Blood, 104 (2004) 3257–3266. [PubMed: 15284116]

[53]. Schlessinger J, Axelrod D, Koppel DE, Webb WW, Elson EL, Lateral transport of a lipid probe and labeled proteins on a cell membrane, Science, 195 (1977) 307–309. [PubMed: 556653]

[54]. Mufson EJ, Brady DR, Kordower JH, Tracing neuronal connections in postmortem human hippocampal complex with the carbocyanine dye DiI, Neurobiol Aging, 11 (1990) 649–653. [PubMed: 1704107]

[55]. von Bartheld CS, Cunningham DE, Rubel EW, Neuronal tracing with DiI: decalcification, cryosectioning, and photoconversion for light and electron microscopic analysis, J Histochem Cytochem, 38 (1990) 725–733. [PubMed: 2185313]

[56]. Pontius WD, Wallace LC, Fife K, Hubert CG, Human Glioblastoma Organoids to Model Brain Tumor Heterogeneity Ex Vivo, in: Seano G (Ed.) Brain Tumors, Springer US, New York, NY, 2021, pp. 133–158.

[57]. Pituch KC, Miska J, Krenciute G, Panek WK, Li G, Rodriguez-Cruz T, Wu M, Han Y, Lesniak MS, Gottschalk S, Balyasnikova IV, Adoptive Transfer of IL13Ralpha2-Specific Chimeric Antigen Receptor T Cells Creates a Pro-inflammatory Environment in Glioblastoma, Mol Ther, 26 (2018) 986–995. [PubMed: 29503195]

[58]. Pituch KC, Zannikou M, Ilut L, Xiao T, Chastkofsky M, Sukhanova M, Bertolino N, Procissi D, Amidei C, Horbinski CM, Aboody KS, James CD, Lesniak MS, Balyasnikova IV, Neural stem cells secreting bispecific T cell engager to induce selective antiglioma activity, Proc Natl Acad Sci U S A, 118 (2021).

[59]. Marquez-Ortiz RA, Contreras-Zarate MJ, Tesic V, Alvarez-Eraso KLF, Kwak G, Littrell Z, Costello JC, Sreekanth V, Ormond DR, Karam SD, Kabos P, Cittelly DM, IL13Ralpha2 Promotes Proliferation and Outgrowth of Breast Cancer Brain Metastases, Clin Cancer Res, 27 (2021) 6209–6221. [PubMed: 34544797]

[60]. Darmanis S, Sloan SA, Croote D, Mignardi M, Chernikova S, Samghababi P, Zhang Y, Neff N, Kowarsky M, Caneda C, Li G, Chang SD, Connolly ID, Li Y, Barres BA, Gephart MH, Quake SR, Single-Cell RNA-Seq Analysis of Infiltrating Neoplastic Cells at the Migrating Front of Human Glioblastoma, Cell Rep, 21 (2017) 1399–1410. [PubMed: 29091775]

[61]. Bligh EG, Dyer WJ, A rapid method of total lipid extraction and purification, Can J Biochem Physiol, 37 (1959) 911–917. [PubMed: 13671378]

[62]. https://biorxiv.org/cgi/content/short/2021.10.15.464284v1, in.

[63]. He C, Sheng L, Pan D, Jiang S, Ding L, Ma X, Liu Y, Jia D, Single-Cell Transcriptomic Analysis Revealed a Critical Role of SPP1/CD44-Mediated Crosstalk Between Macrophages and Cancer Cells in Glioma, Front Cell Dev Biol, 9 (2021) 779319. [PubMed: 34805184]

[64]. Chen Z, Feng X, Herting CJ, Garcia VA, Nie K, Pong WW, Rasmussen R, Dwivedi B, Seby S, Wolf SA, Gutmann DH, Hambardzumyan D, Cellular and Molecular Identity of Tumor-Associated Macrophages in Glioblastoma, Cancer Res, 77 (2017) 2266–2278. [PubMed: 28235764]

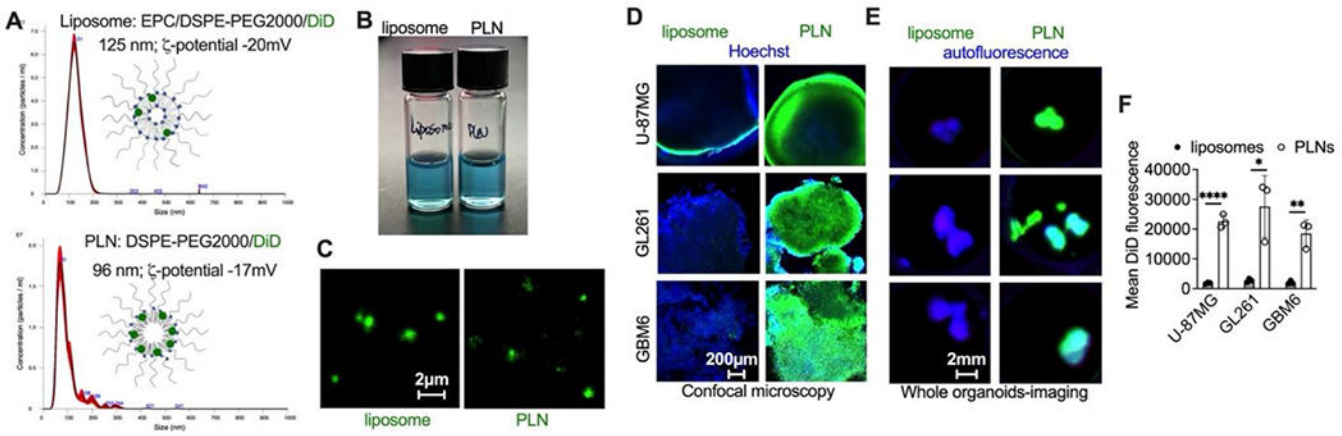

Fig. 1. PLN-formulated ICLs penetrate glioma organoids more efficiently than liposomal ICLs.

A) PEGylated liposomes and PLNs (formulated with 0.4 mol% and 30 mol% DiD, top and bottom, respectively); **B**) both formulations are colloidally stable; **C**) confocal microscopy images of liposomes and PLNs. While the nanoparticle size cannot be accurately estimated by microscopy due to the diffraction limit, both particle types are smaller than 1μm. Sizer bar is the same for both images; **D-E**) penetration of PLN-formulated DiD but not liposomal DiD in glioma spheroids (U-87MG) and tumor organoids (GL261 and GBM6). Particles and liposomes were added at 0.7μM DiD for 24h. Organoids and explants were fixed and imaged with a confocal microscope (D) or Bio-Rad gel imager (E). The confocal depth (Z-plane) was 50-100μm from the spheroid surface for all experiments; **F**) quantification of DiD fluorescence from images in (E). N=3 organoids per group; 2-tailed parametric t-test. P-value: ****<0.0001, **<0.01, *<0.05.

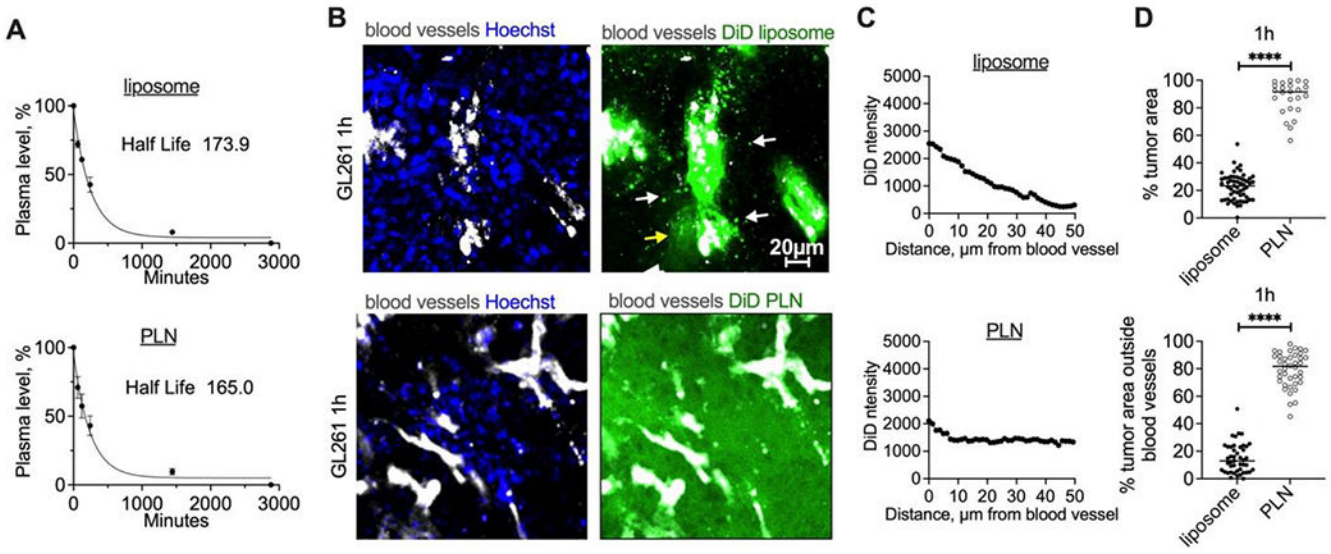

Fig. 2. PLN-formulated ICLs extravasate glioma tumors more efficiently than liposomal ICLs.

PLNs or liposomes were injected i.v. (0.14 μmol DiD/kg); **A**) Circulation half-life of PLN or liposomal DiD (n=3 mice); **B**) representative confocal images (from 3 mice per group) of fresh tumor slices at 1h post-injection of liposomal and PLN-formulated DiD (mice were perfused postmortem to remove the blood); **C**) line profiles drawn across representative blood vessels show much more efficient spreading of PLN-formulated DiD than liposomal DiD; **D**) quantification of fluorescence-positive areas (top) and extravascular fluorescence areas (bottom) in fresh tumor slices of PLN DiD-injected mice (N=3 mice per group, 2-tailed parametric t-test). P-value: ****<0.0001.

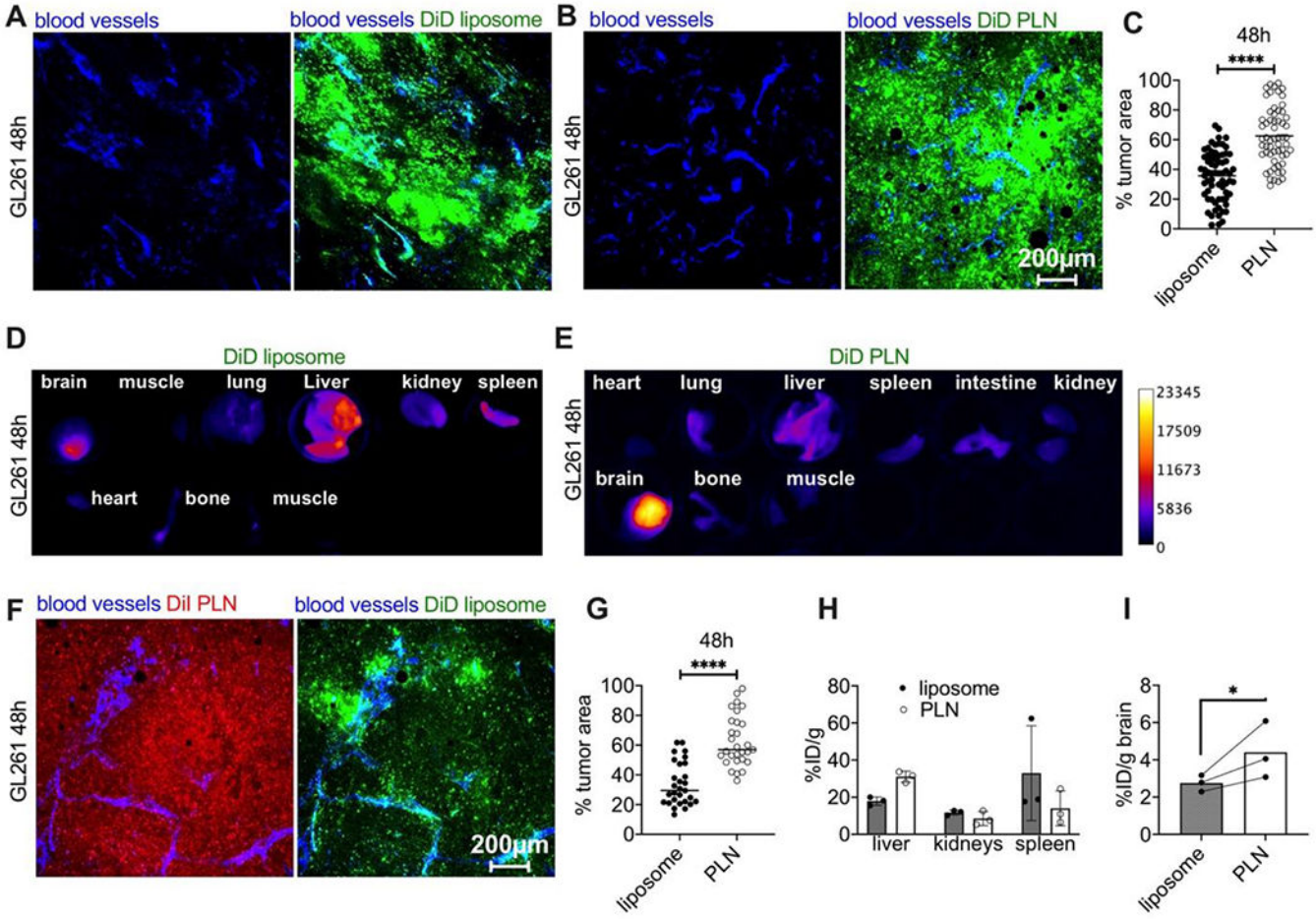

Fig. 3. PLN-formulated ICLs accumulate in gliomas at 48h more efficiently than liposomal ICLs.

A-B) Representative *ex vivo* confocal microscopy images (from 3 mice per group) of tumor slices from mice injected with liposomal DiD or PLN-formulated DiD. Scale bar is the same for all images; **C**) quantification of % fluorescent area in tumors (n=3 mice per group, pairwise t-test); **D-E**) pseudocolored images of DiD fluorescence in main organs after injection of liposomal DiD or PLN-formulated DiD; **F**) representative confocal microscopy images of tumor (central area) after co-injection of PLN-formulated DiI (Supplemental Fig. 2) and liposomal DiD; **G**) quantification of tumor's fluorescent area after co-injection of DiI PLN and DiD liposomes (n=3 mice per group, pairwise t-test); **H-I**) accumulation (% ID/g) of liposomal and PLN-formulated ICLs after extraction from clearance organs and brains of GL261 tumor-bearing mice. N=3 mice, pairwise t-test. P-value: ****<0.0001; *=0.04.

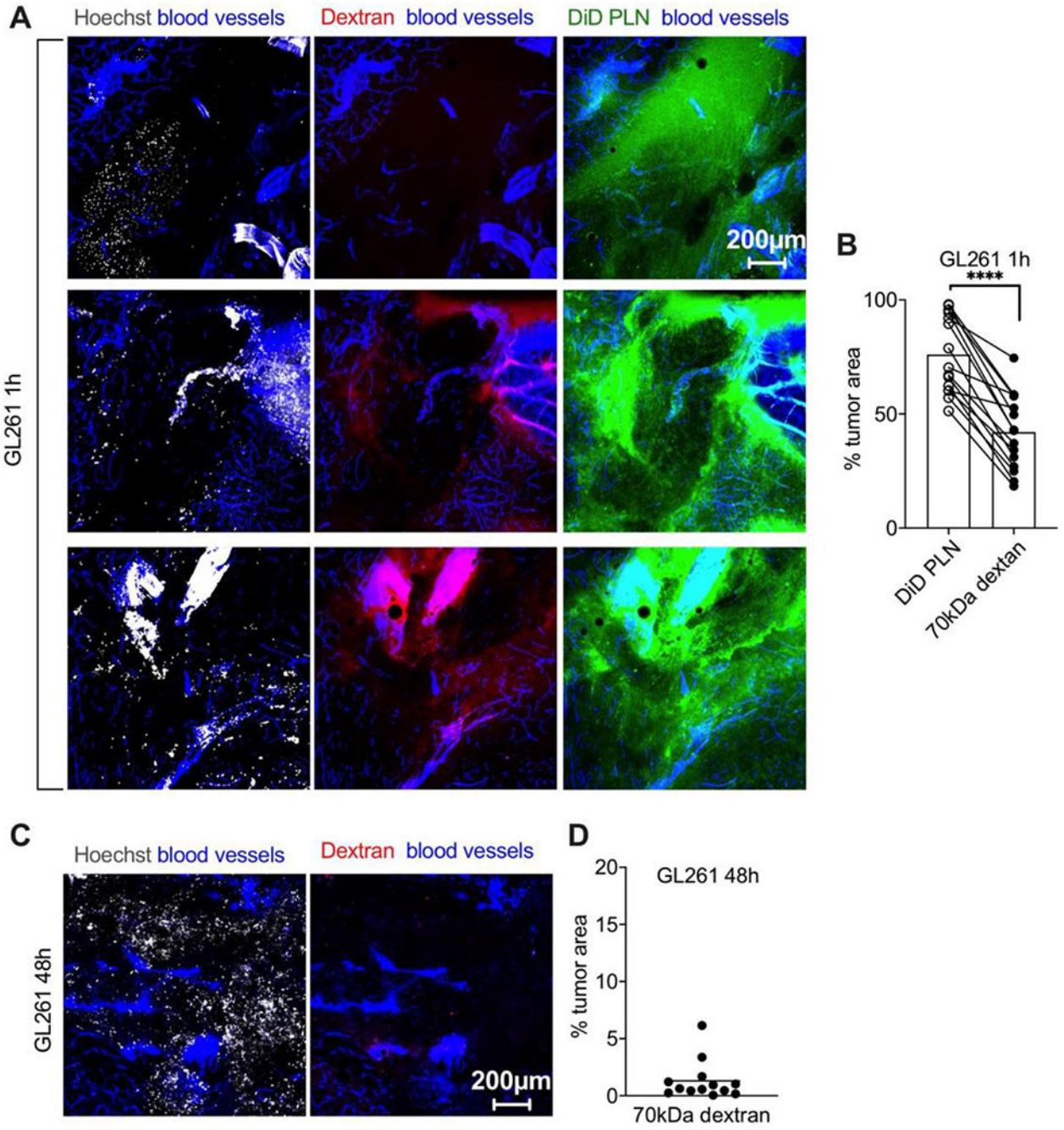

Fig. 4. PLN-formulated ICLs extravasate and accumulate in gliomas more efficiently than 70kDa rhodamine-dextran.

GL261 tumor-bearing mice were co-injected with DiD PLN and rhodamine dextran (0.14 and 0.33 μmol dye/kg, respectively). **A**) Representative confocal images of different areas of fresh non-fixed GL261 tumor slices show superior extravasation of PLN-formulated DiD over dextran injected in the same mice; **B**) quantification of % tumor fluorescent area (n=3 mice per group, pairwise t-test. P-value: ****<0.0001); **C-D**) minimal accumulation of

rhodamine dextran at 48h injected in a separate cohort of GL261 tumor-bearing mice (n=3 mice per group).

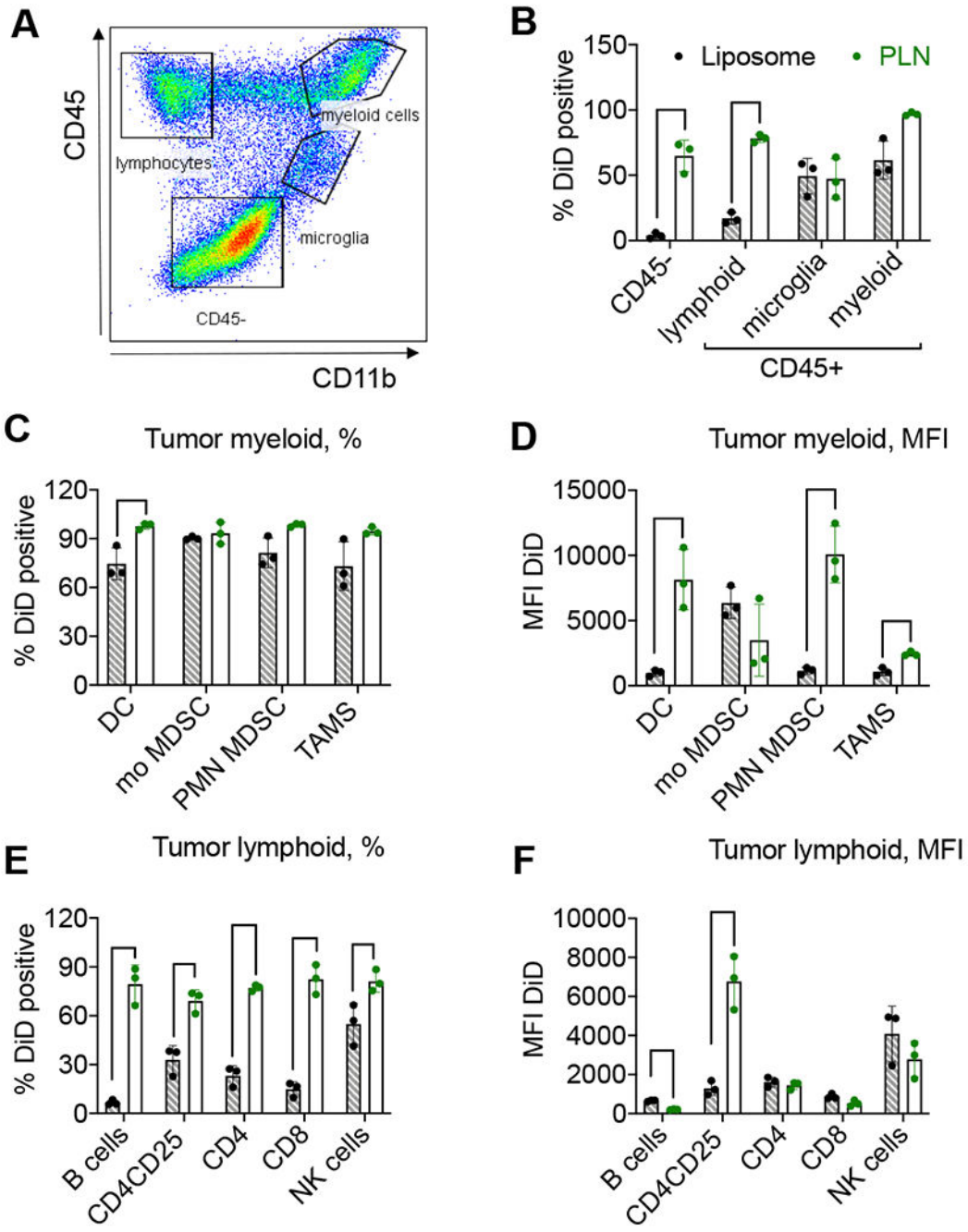

Fig. 5. Flow cytometry analysis demonstrates better accumulation of PLN-formulated DiD than liposomal DiD.

GL261 tumor-bearing mice were injected with DiD liposomes or DiD PLNs, and the cell uptake was analyzed 48h post-injection. **A**) Gating strategy (also Supplemental Figs. 4–6); **B**) CD45+ and CD45− populations (% or cells). Bar labels are the same for all subsequent graphs; **C**) myeloid cell subtypes (% or cells); **D**) myeloid cell subtypes (mean fluorescence intensity, MFI); **E**) lymphoid cell subtypes (% of cells); **F)** lymphoid cell subtypes (MFI). Dendritic cells (DC), monocytic MDSCs (mo MDSC), polymorphonuclear

MDSC (PNM MDSC), and tumor-associated macrophages (TAMs). N=3 mice per group, parametric t-tests with multiple comparisons. Only significant comparisons are indicated. P-value: ****<0.0001; ***<0.001, **<0.01, *<0.05.

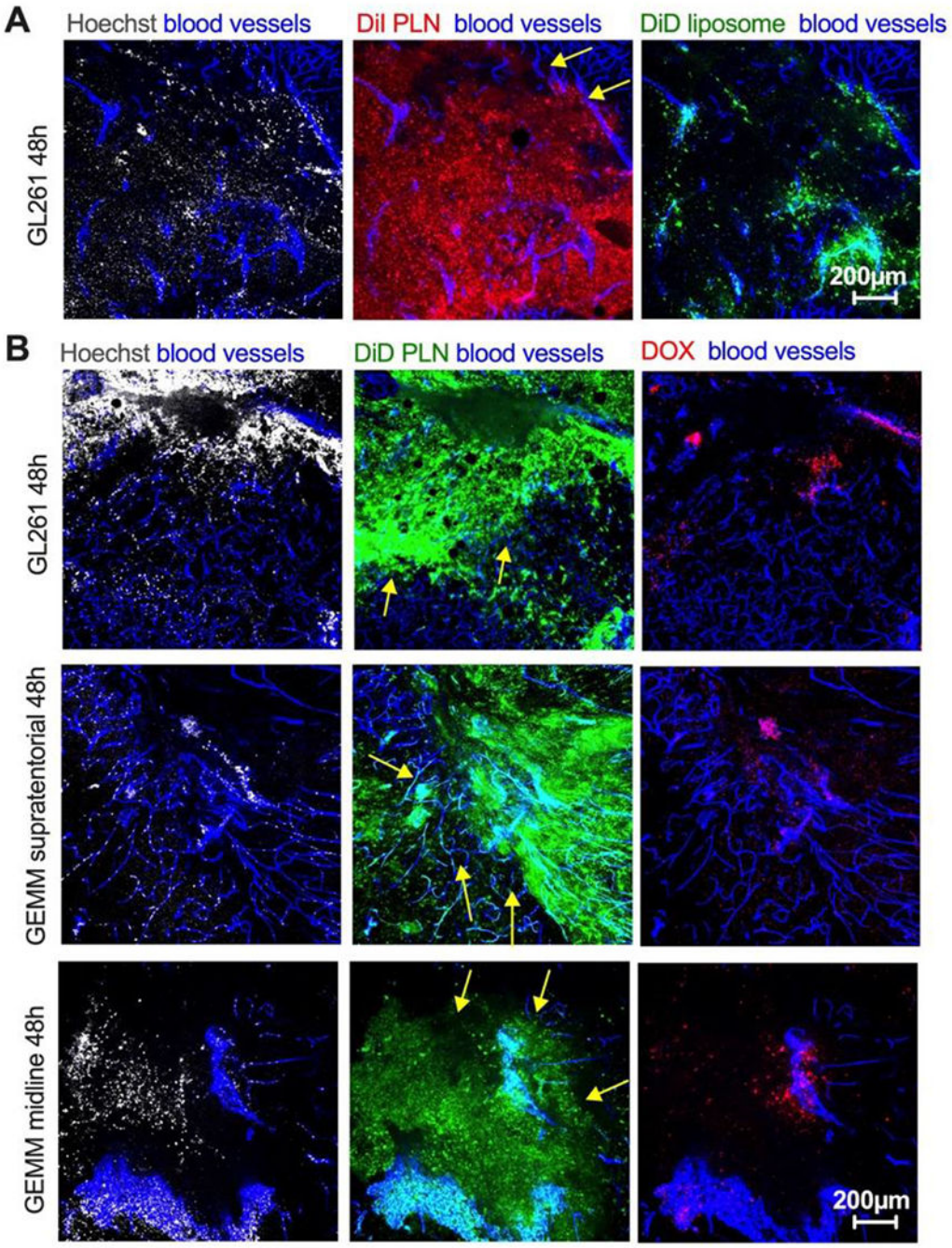

Fig. 6. Localization of PLN-formulated ICLs in tumor margin 48h post-injection.

Mice were injected and imaged as described in Fig. 3. **A**) DiI PLN and DiD liposomes were coinjected in GL261 mice. Difference in the margin (arrows) localization between PLN-formulated DiI and liposomal DiD in GL261 tumor; **B**) PLN-formulated DiD and PEGylated liposomal doxorubicin (DOX) were coinjected in GL261 mice (top row) and in genetically engineered invasive mouse models (supratentorial high-grade and diffuse midline glioma, middle and bottom rows). Arrows point to the margin. The size bar is the same for all images. The experiment is repeated twice.

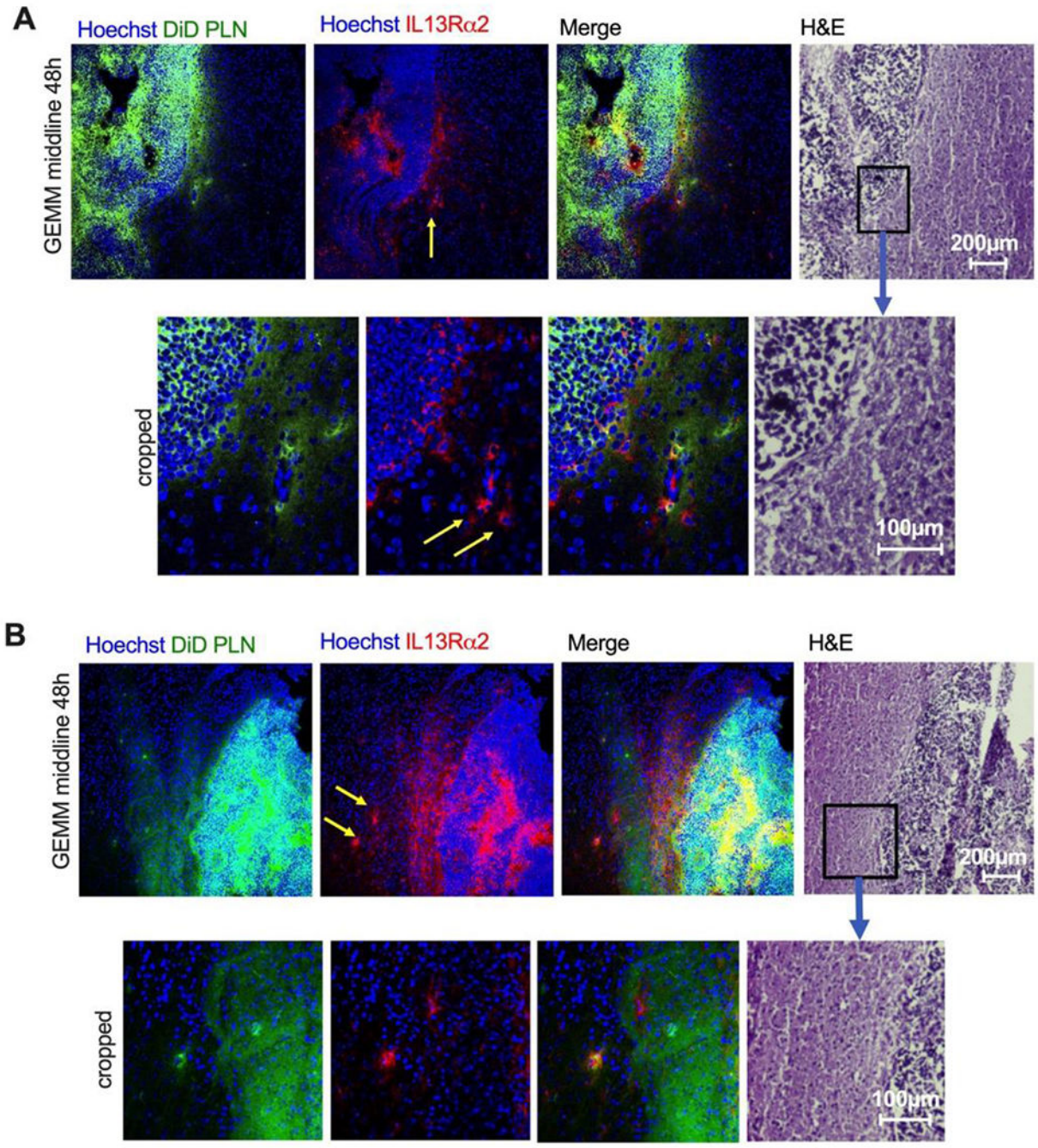

Fig. 7. Localization of PLN-formulated ICLs in brain-invading cells 48h post-injection.

A-B) Representative high-magnification fields of diffuse midline glioma GEMM with engineered human IL13Rα2 receptor 48h after injection of PLN-formulated DiD. Immunostaining for IL13Rα2 was used to identify tumor cells. In addition, sequential H&E staining is shown to confirm the tumor edge. There was colocalization of DiD with the invasive margin and some of the breakaway cells (yellow arrows).

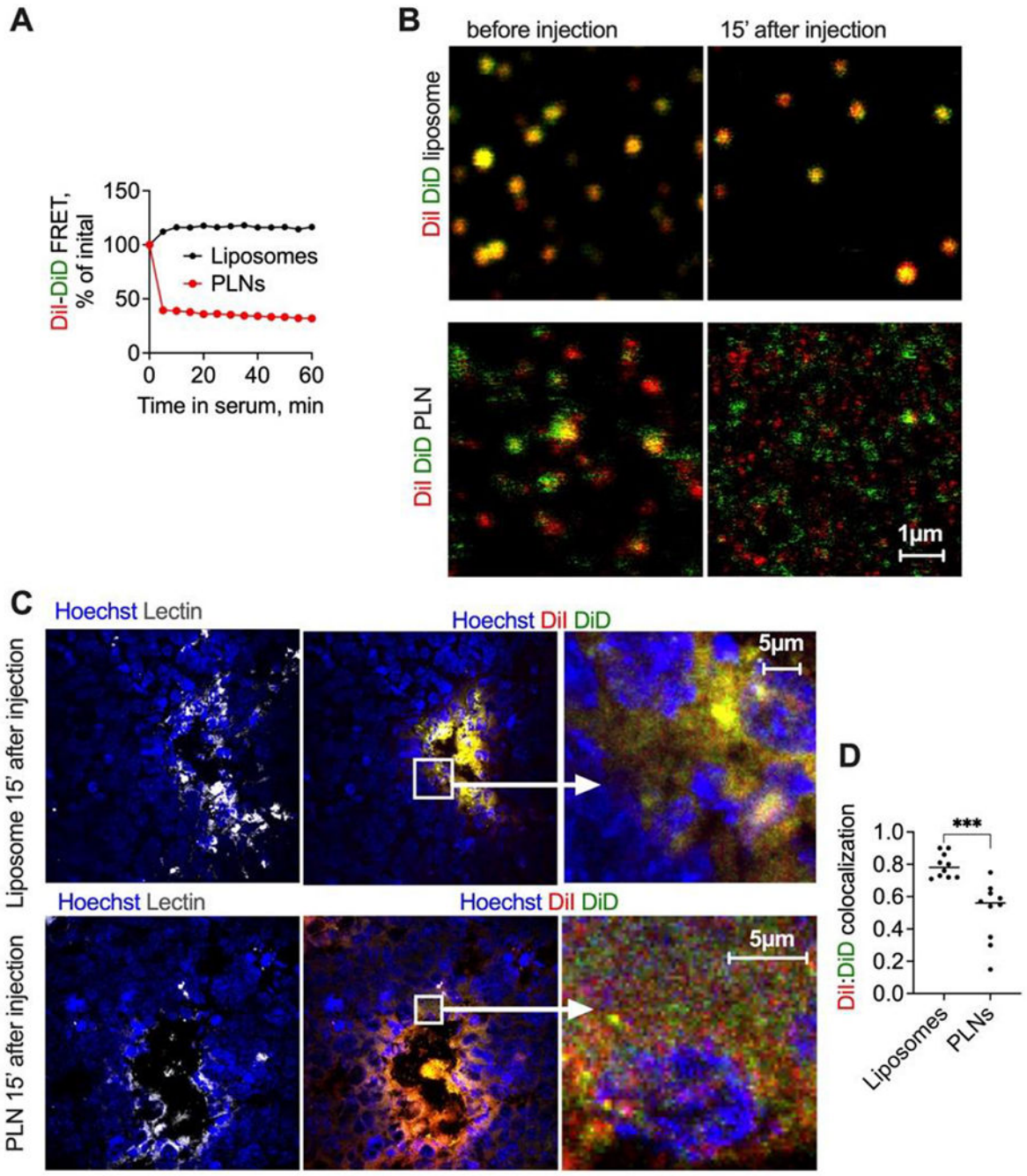

Fig. 8. PLNs show instability in serum in vitro and in vivo.

A) Normalized FRET efficiency (Supplemental Fig. 9 for absolute FRET values) after incubation of double-labeled PLNs and liposomes in mouse serum; **B**) confocal microscopy in plasma post-injection shows the disintegration of PLNs and stability of liposomes. The size bar is the same for all images; **C**) high magnification microscopy of GL261 tumor histological sections show a separation of PLN-formulated DiI/DiD, but not liposomal

DiI/DiD at early steps of tumor entry; **D**) colocalization of DiI and DiD in PLN injected tumors and in liposome-injected tumors (Pearson coefficient, calculated with Coloc2 in Fiji).